Vol. 23, n.°4, pp. 57-68, 2024
Revista UIS Ingenierías
https://revistas.uis.edu.co/index.php/revistauisingenierias

Dual Polarization Optical Slicing for C-RAN in 5G Networks based on Radio-over-Fiber

Particionado óptico de doble polarización para C-RAN en redes 5G basadas en Radio-sobre-Fibra

Gustavo Adolfo Puerto Leguizamón [1a], Carlos Arturo Suárez Fajardo [1b]

[1] Facultad de Ingeniería, Universidad Distrital Francisco José de Caldas, Colombia. Orcid: 0000-0002-6420-9693 [a], 0000-0002-1460-5831 [b]. Email: gapuerto@udistrital.edu.co [a], csuarezf@udistrital.edu.co [b].

Received: 23 April 2024. Accepted: 26 August 2024. Final version: 23 November 2024.

Abstract

This paper investigates the potential of a dual polarized optical spectral slicing system to enable high-capacity optical links in the Cloud-Radio Access Network (C-RAN) segment based on Radio-over-Fiber (RoF) of a 5G network. The process of signal generation based on optical slicing with dual polarization is described analytically and a conducted experimental demonstration is performed to assess the feasibility of the proposal. Experimental results focus on the Error Vector Magnitude (EVM) measurements for 0.1 nm, 0.5 nm, and 1 nm dual polarized optical slices. Data is experimentally measured for QPSK and 64QAM signals at 1.7 GHz and 3.5 GHz carrier frequencies across 10 km of single mode optical fiber. The results demonstrate that the 0.1 nm optical slice with QPSK at 1.7 GHz leads to an EVM of 2.4%, while an EVM of 4.5% is observed for 64QAM under the same conditions. Additionally, simulation modeling projects the feasibility of RoF transport of 64QAM signals at 1.7 GHz and 3.5 GHz over 25 km and 16 km fiber links respectively.

Keywords: Optical spectral slicing; fronthaul; 5G; Optical signal generation; Radio-over-Fiber.

Resumen

Este artículo investiga el potencial de un sistema de particionado espectral óptico de doble polarización para permitir enlaces ópticos de alta capacidad en el segmento de la red de acceso a radio en la nube (C-RAN, *Cloud-Radio Access Network*) basados en radio sobre fibra (RoF, *Radio-over-Fiber*) de una red 5G. Se describe analíticamente el proceso de generación de señal basado en particionado óptico con polarización dual y se realiza una demostración experimental para evaluar la viabilidad de la propuesta. Los resultados experimentales se centran en medir la magnitud del vector de error (EVM, *Error Vector Magnitude*) para ranuras ópticas de doble polarización de 0.1 nm, 0.5 nm y 1 nm. Los datos se miden experimentalmente para señales QPSK y 64QAM en frecuencias portadoras de 1.7 GHz y 3.5 GHz en 10 km de fibra óptica monomodo. Los resultados demuestran que una partición óptica de 0.1 nm con QPSK a 1.7 GHz conduce a un EVM de 2.4%, mientras que para 64QAM se observó un EVM del 4.5% bajo las mismas condiciones. Además, el modelo de simulación proyecta la viabilidad del transporte RoF de señales 64QAM a 1.7 GHz y 3.5 GHz en enlaces de fibra de 25 km y 16 km respectivamente.

Palabras clave: Particionado espectral; fronthaul; 5G; generación de señal óptica; Radio-sobre-Fibra.

ISSN Online: 2145 - 8456

How to cite: G. A. Puerto Leguizamón, C. A. Suárez Fajardo, “Dual Polarization Optical Slicing for C-RAN in 5G Networks based on Radio-over-Fiber,” *Rev. UIS Ing.*, vol. 23, no. 4, pp. 57-68, 2024, doi: https://doi.org/10.18273/revuin.v23n4-2024005

1. Introduction

The boundless ambition of 5G wireless networks and beyond envisions a future of lightning-fast speeds, ubiquitous connectivity, and transformative applications that demand ultra-low latency and low power consumption [1]. To achieve this vision, a paradigm shift in network architecture is required. Radio-over-Fiber (RoF) technology bridges the fields of wireless and optical communications, providing a powerful solution to many of the challenges presented by 5G [2]. The ability of RoF to distribute high-bandwidth, low-latency signals over fiber links makes it indispensable for fronthaul networks, which is the network segment that connects the centralized baseband processing units (BBUs) to the Remote Radio Heads (RRHs) [3].

Within the Cloud-Radio Access Network (C-RAN) the way optical carriers are generated to transport radio signals significantly impacts both performance and operational cost. Traditional RoF systems often rely on a dedicated laser source for each radio frequency (RF) channel. However, in dense 5G networks characterized by small cells, this approach becomes complex and economically inefficient [4]. In this context, the use of optical frequency comb techniques has emerged as a key feature to enable applications such as spectroscopy [5], development of spectrally-efficient and adaptable optical transceivers [6], [7], [8] signal generation in mm-Wave and Terahertz bands [9], [10], [11], [12], [13] and radio-over-fiber systems [14]. These applications exploit the inherent characteristics of frequency combs such as their high mutual coherence and fixed frequency spacing among generated carriers to enable system advantages that would otherwise not be possible when relying on multiple independent lasers.

In such a context, optical slicing emerges as an alternative for carrier generation, offering a way to produce multiple optical carriers from a single broadband light source. By applying carefully selected optical filters, the optical spectrum can be efficiently sliced into individual carrier signals. The characteristics of the filter determine the frequency, power and linewidth of the generated carriers. In addition, the exploitation of the polarization domain for each one of the generated carriers enables an increased capacity with improved spectral efficiency and flexibility to transport different service profiles using the same optical sliced carrier [15], [16], [17].

While promising, optical spectral slicing necessitates a thorough understanding of its impact on signal quality. The key lies in the trade-off between the bandwidth of the optical filter and the modulation characteristics of the RF signal. It should be pointed out that optical spectral slicing, while potentially minimizes costs and complexity, also may be a source of signal distortion and it may jeopardize the spectral efficiency, particularly for the densely modulated signals characteristic of 5G. This trade-off between the achievable signal quality and optimal use of spectrum underscores the need for careful analysis to ensure spectral slicing meets the strict demands of the 5G C-RAN network. Therefore, the motivation of this work lies in the need to find a way of minimizing infrastructure costs while simplifying the manner in which a wavelength channel can be generated and used in the 5G C-RAN network segment.

In this work, the analysis and performance of a dual polarized optical slicing based on optical filtering of a broadband optical source for the transport of RoF is assessed. The conducted evaluation is based on Error Vector Magnitude (EVM) measurements of service profiles transported in Quadrature Phase Shift Keying (QPSK) and 64 Quadrature Amplitude Modulation (64QAM) modulation formats onto 1.7 GHz, also known as the Advanced Wireless Services (AWS), and 3.5 GHz. These frequencies belong to two of the frequency bands considered for the 5G deployments worldwide.

Unlike the previous works, this proposal demonstrates the transport of dual polarized optical carriers for RoF featuring 0.1 nm, 0.5 nm and 1 nm linewidths. These values are wider than the typical commercial linewidth lasers whose characteristics features linewidths that ranges from 0.0001nm to 0.5 nm [18], [19]. This characteristic enables profitable and low power consumption RoF transport of signals covering the typical distances of a 5G C-RAN. To the best of our knowledge, this proposal represents the first demonstration of a dual polarized transport based on optical slicing. The paper is organized as follows: In Section II, the analytical description of the optical slicing with dual polarization technique and the description of the experimental implementation are presented. Section III describes the experimental and simulation results of the proposed approach and finally the conclusions are given in Section IV.

2. Methods

2.1. Analytical description

A Semiconductor Laser Amplifier determines the structure of a broadband optical source. Equation (1) provides the gain of such a structure as:

$$G = e^{(\Psi c - \alpha)L} \tag{1}$$

Where ψ_c is the confinement factor, α determines the losses of the active zone and L is the cavity length of the laser. If R is the reflectivity of the cavity sidewalls, the transfer function of a broadband optical source, according to [20] is defined in Equation (2) as:

$$G(\upsilon) = \frac{(1-R_1)(1-R_2)G}{(1-G\sqrt{R_1R_2})^2 + 4G\sqrt{R_1R_2}sin^2\left(\pi\frac{\upsilon-\upsilon_m}{\Delta\upsilon_L}\right)} \quad (2)$$

Where υ is the emission frequency of the optical source, υ_m with m = 1, 2, 3, …n, are the periodic resonance frequencies of the optical source and $\Delta\upsilon_L = c/2nL$ is the separation between such resonances. A broadband optical source generates a sufficiently wideband spectrum when the Contrast Ratio (CR) is less than 2, CR is defined as the ratio of maximum and minimum gain of the laser amplifier and is given by Equation (3)

$$CR = \left(\frac{1+G\sqrt{R_1R_2)}}{1-G\sqrt{R_1R_2)}}\right)^2 \quad (3)$$

Thus, the condition for the generation of a wideband spectrum implies that:

$$G\sqrt{R_1R_2)} < 0.17 \quad (4)$$

Therefore, for a typical gain of a laser amplifier of 20 dB, the reflectivity R of the cavity sidewalls is given by Equation (5) as:

$$\sqrt{R_1R_2)} < 1.7x10^{-3} \quad (5)$$

This indicates that the reflectivity R must be as low as possible in order to enable a gain spectrum with a wide broadband response.

As far as the optical filtering to perform the optical slicing of the broadband source is concerned, the approach makes use of an Arrayed Waveguide Grating which is a planar multiplexer-demultiplexer that is a generalization of the Mach-Zehnder interferometer [21]. The filter is based on the use of two identical NxM planar couplers in mirror configuration to interconnect and interfere the signals coming from N planar waveguides as described in [22]. The transfer function of the filter that characterizes the input by the waveguide p and the output by the waveguide q can be expressed as:

$$T_{pq} = \frac{\left|\sum_{r=1}^{M} Ge^{j\phi r}\right|^2}{G^2} \quad (6)$$

Where G represents the power of the broadband source in the waveguide p, as described in equation (2), and ϕ the phase imposed by the waveguide r that connects the two couplers. The length of the waveguides that connects the two couplers determines the phase ϕ_r for each waveguide r. If the propagation constant in all of the waveguides is β, and ρ, ρ' represent the angular separation between the guides at the input of the first coupler and the separation between the guides at the output of the first coupler respectively, the difference in length between adjacent guides i.e. r and $r + 1$ is fixed with a value l, then the phase difference between adjacent guides is independent of the value of r, obtaining Equation (7) and Equation (8) as:

$$\Delta\phi = \phi_{k+1} - \phi_k = \beta l + k_0 n_1 R(p-q)\rho\rho' \quad (7)$$

Then,

$$\Delta\phi(\lambda) = \frac{2\pi n_1 n_{eff} l}{\lambda} + \frac{2\pi n_1}{\lambda} R(p-q)\rho\rho' \quad (8)$$

Where R is the focal length, $k_0 = 2\pi/\lambda$ and n_{eff} is the effective refractive index of the guide that connects both couplers. The first addend describes the incremental phase change undergone by the signal in the waveguide and the second one includes the phase changes due to the propagation in the unguided areas of the couplers that have a refractive index n_1. By using equation (8) in equation (6), the transfer function for the optical filter is expressed in Equation (9) as:

$$T_{pq}(\Delta\phi) = \varepsilon_p\varepsilon_q|h(\Delta\phi)|^2 \quad (9)$$

With

$$h(\Delta\phi) = \frac{\sum_{r=1}^{M} Ge^{j\Delta\phi r}}{\sum_{r=1}^{M} G} \quad (10)$$

$\varepsilon_p\varepsilon_q$ is the transfer efficiency of the filter, i.e. the ratio of the power between the outputs and inputs of the two planar couplers respectively. The response described in equation (10) depends on the signal wavelength and its maximum value corresponds to $\varepsilon_p\varepsilon_q$ that is obtained for a wavelength value $\bar{\lambda}$ that verifies the condition:

$$\frac{2\pi n_1 n_{eff} l}{\bar{\lambda}} + \frac{2\pi n_1}{\bar{\lambda}} R(p-q)\rho\rho' = 2m\pi \quad (11)$$

With $m = 0 \pm 1 \pm 2$ ⋯. Equation (11) indicates that the transfer function given by equation (10) corresponds to a periodic wavelength filter. Such periodic response enables the optical passbands that define the linewidth of an optical carrier. By considering two adjacent waveguides at the output of the device, e.g. $q=0$ and $q=1$ the difference between the phases that produce maximum values at the output of each one of them can be obtained from equation (8) as:

$$\Delta\phi_{10} = \Delta\phi_{\substack{p=0\\q=1}} - \Delta\phi_{\substack{q=0\\q=1}} = \frac{2\pi n_1 R}{\lambda}\rho\rho' \qquad (12)$$

$\Delta\phi_{10}$ corresponds to the wavelength spacing of the resonances chosen by adjacent outputs, i.e. $q = 0$ and $q = 1$. This spacing dictates the minimum frequency separation of the adjacent channels at the output of the optical filter. On the other hand, the free spectral range in phase units of any of the configurations T_{pq} is 2π. Consequently, the maximum number of channels that the filter can demultiplex is given by Equation (13) as:

$$N = \frac{2\pi}{k_0 n_1 R\rho\rho'} = \frac{\lambda}{n_1 R\rho\rho'} \qquad (13)$$

The passband width, i.e. the linewidth, for each resonance of the filter obtained at -3dB is given by equation (14) as $|h(\Delta\varphi)|^2$.

$$|h(\Delta\emptyset)^2| = \frac{sin^2(\frac{\Delta\emptyset}{2})}{Nsin^2(\frac{\Delta\emptyset}{2})} \qquad (14)$$

Regarding the polarization treatment of the generated signal, it is well-known that an arbitrary state of polarization of an electrical field can be split up as an addition of two orthogonal states of polarization. The envelope of such electric field is described by:

$$E = E_x\hat{x} + E_y\hat{y} = a_x e^{j\varphi_x}\hat{x} + a_y e^{j\varphi_y}\hat{y} \qquad (15)$$

Where $\hat{x}$ and $\hat{y}$ represent the unit vectors in x and y directions. Then, any polarization state can be expressed by a two component Jones vector as:

$$J = \begin{pmatrix} E_x \\ E_y \end{pmatrix} = \begin{pmatrix} a_x e^{j\varphi_x} \\ a_y e^{j\varphi_y} \end{pmatrix} \qquad (16)$$

In such a context, if J_i and J_o are respectively the Jones vectors of the polarization states at the input and output of the polarization beam splitter, the Jones matrix M that relates inputs and outputs of such device is given by:

$$M = \begin{pmatrix} 1 & 0 \\ 0 & 0 \end{pmatrix} + \begin{pmatrix} 0 & 0 \\ 0 & 1 \end{pmatrix} \qquad (17)$$

The first and second addends represent the Jones matrix of the horizontal polarization state and vertical polarization state respectively. Since $J_o = M \cdot J_i$, the output of the polarization beam splitter based on (16) and (17) is expressed as:

$$\begin{pmatrix} E_x^o \\ E_y^o \end{pmatrix} = \begin{pmatrix} 1 & 0 \\ 0 & 0 \end{pmatrix} \cdot \begin{pmatrix} E_x^i \\ E_y^i \end{pmatrix} + \begin{pmatrix} 0 & 0 \\ 0 & 1 \end{pmatrix} \cdot \begin{pmatrix} E_x^i \\ E_y^i \end{pmatrix} \qquad (18)$$

2.2. Implementation Details

Figure 1 shows the layout of the experimental setup in which a broadband laser source to generate an optical signal ranging from 1000 nm to 2000 nm was used. Then, this wideband signal feeds an optical filter that is centered at 1550 nm. The purpose of this filter is to slice portions of spectrum from the broadband signal in order to obtain the corresponding passbands. In this proposal, the optical filter is configured with passband widths of 0.1 nm, 0.5 nm and 1 nm. The purpose of these passbands is to determine the linewidth of the optical slice that will act as optical source to feed the polarization beam splitter (PBS). Then, the PBS separates the optical slice into two orthogonal polarized signals, xPol and yPol, where each polarized signal is used to feed an electro-optic modulator (EOM) that receives the information signals of the arbitrary waveform generator (AWG). In this context, a vector network analyzer (VNA) was also employed to provide a radio frequency bandwidth from 5 MHz up to 5 GHz to the system in order to characterize the behavior of the system in a wide frequency spectrum.

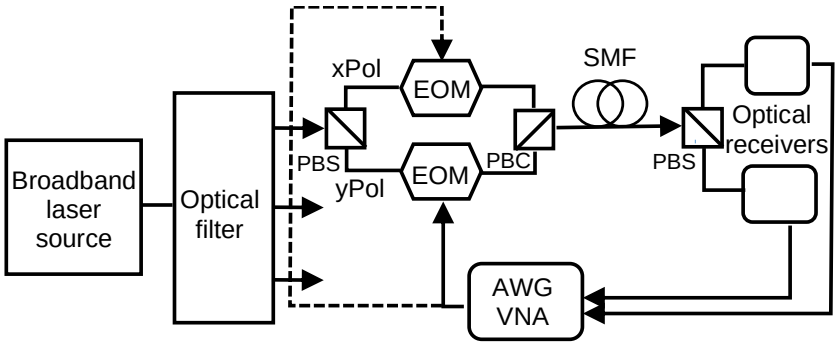

Figure 1. Experimental setup for the transport of optical slices with dual polarization signals. Source: Own elaboration.

It should be pointed out that Frequency Range 1 (FR-1) band of 5G is included in the evaluated radio frequency bandwidth. Subsequently, both orthogonal channels are multiplexed in the polarization beam combiner (PBC) and launched to the optical single mode fiber (SMF) link. The experiments included optical links of 1 km, 5 km and 10 km lengths. The performance was assessed under various propagation conditions by testing the system over different link lengths. Next, after RoF signals propagation through the fiber, an optical receiver was used to convert the optical signal back into an electrical signal to perform the measurements and assess the system performance in both the AWG and the VNA.

3. Results

3.1. Experimental results

Figure 2 shows the spectra of the dual polarized sliced carriers measured at the output of the PBS. Figure 2(a) show the orthogonal components for a slice linewidth of 0.1 nm, Figure 2(b) shows the polarized components for a slice of 0.5 nm and Figure 2(c) shows the slice linewidth of 1 nm.

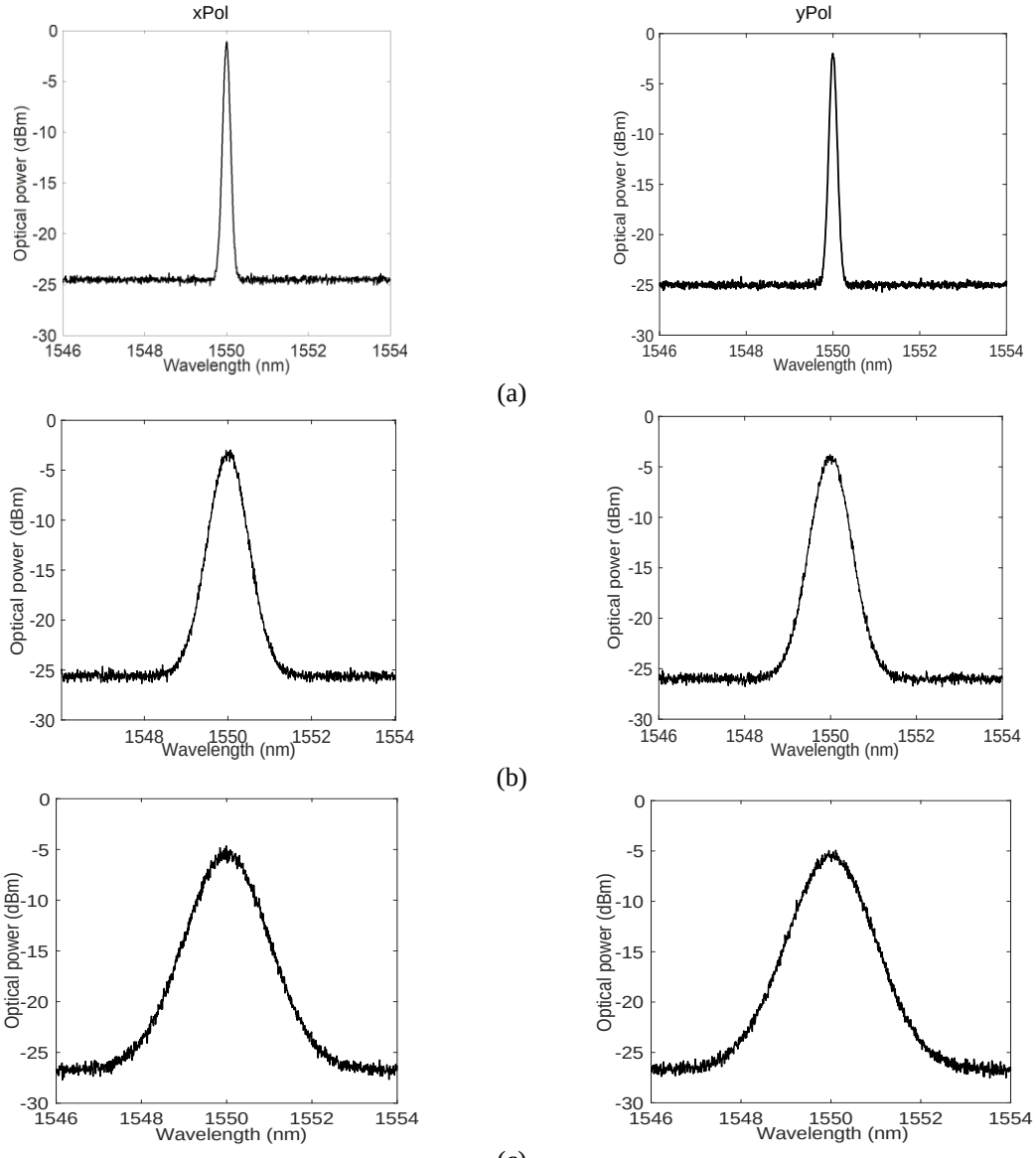

Figure 2. Experimental results: 2(a) xPol and yPol for 0.1 nm optical slice. (b) xPol and yPol for 0.5 nm optical slice. (c) xPol and yPol for 1 nm optical slice. Source: Own elaboration.

The responses depicted in Figure 2 show how the phase difference between the waveguides inside the optical filter expressed in Equation (8) impacts the transfer function presented in Equation (9), particularly on the passband width of the optical filter described in Equation (14).

The PBS featured an extinction ratio of 40 dB, this value assures a splitting process suitable for this proposal. However, as it can be observed, slight differences in power and noise floor were found in the measurements. The observable differences arise from the polarized signal beat between the outputs of the PBS as predicted by the Jones matrix of the PBS presented in Equation (18). It means that there is a remnant of the xPol signal that goes to the yPol output of the PBS generating coherence around the center wavelength in the optical receiver. The same effect occurs from the yPol signal to the xPol output.

The characterization of the optical power at different distance propagations for the dual polarized optical slices is shown in Figure 3. In such a context, yPol presents a slight higher power penalty than xPol due to the polarization signal beat for all the evaluated propagation lengths. Also, it was found that the narrower the optical slice the higher the optical power and the higher the optical slice the lower the power available per optical channel. This fact comes directly from the response of the optical filter due to the efficiency terms of the transfer function presented in Equation (9). These terms determine the power penalties for each output port of the filter. However, notice that the power penalty at 10 km increases for optical slices wider than 0.5 nm. This fact comes up from a wider broadening of the optical pulses caused by the chromatic dispersion on both polarized components. Overall, these results demonstrate the feasibility of the approach since no additional penalties were found for each orthogonal component transmitted over different fiber spans, e.g. penalties derived from the fiber birefringence or polarization mode dispersion (PMD).

Figure 4 shows the bandwidth modulation as a function of the optical slice at different lengths. The characterization of the bandwidth modulation is important because it gives information about the range of radio frequency signals that are feasible to transport in our approach. The measurement was performed in the VNA, in which the receiver power at -3 dB was measured for radiofrequency signals from 5 MHz to 5 GHz at different optical slices. It was found a bandwidth of 4.55 GHz for 0.1 nm and 1 km fiber spam. Longer fiber spans reduces the bandwidth due to the combined effect of the slice linewidth and the cumulative dispersion on the fiber link. It should be pointed out that the bandwidth modulation is reduced if the optical slice linewidth is increased. In particular, we found that the approach is able to transport frequencies in the band of 1.7 GHz over 10 km with an optical slice linewidth of 0.95 nm. For the transport of frequencies in the band of 3.5 GHz, the same distance can be covered with a slice linewidth of 0.2 nm. It means that wider slices penalize the system performance due to the chromatic dispersion, so that narrower slices are preferred for the transport of higher frequencies. At this point it is worth to point out that no dispersion compensation process was performed, which implies that the results for fiber spans longer that 10 km can be improved and the bandwidth limitation imposed by optical slices wider than 0.2 nm can be reduced enabling the transport of radiofrequency carriers at 3.5 GHz.

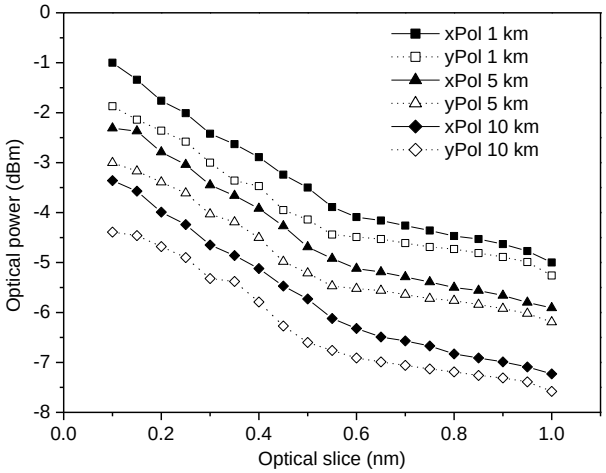

Figure 3. Experimental results: Power at the output of the transmitter as a function of the available pass band. Source: Own elaboration.

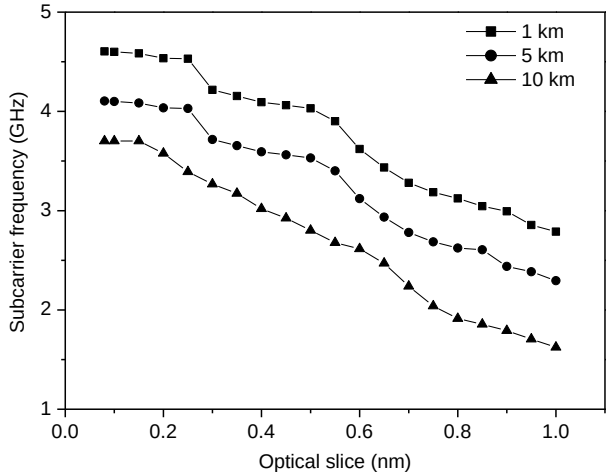

Figure 4. Experimental results: Measured bandwidth for dual polarized optical slices. Source: Own elaboration.

As far as signal quality is concerned, the received constellations after propagation of the information signals in both xPol and yPol components through 10 km of optical fiber were measured. The information signals consist of QPSK and 64QAM signals modulated onto a 1.7 GHz and 3.5 GHz radiofrequency carriers. It is worth to point out that these carriers corresponds to frequencies in the AWS band at 1.7 GHz and the 3.5 GHz band. These bands are of primary importance for the deployment of 5G New Radio (NR) networks in the sub-6 GHz frequencies also known as Frequency Range 1 (FR1).

Figure 5 shows the constellations for a QPSK signal transported in xPol featuring 0.1 nm and 1 nm optical slice linewidths onto 1.7 GHz. The measured Error Vector Magnitude (EVM) of the corresponding constellations transported in optical slices of 0.1 nm and 1 nm was 2.4% and 4% respectively. Both, the EVM and the constellations were measured in the AWG signal analyzer MS2830A. Figure 5 also shows the constellations for a 64QAM signal transported in yPol with 0.1 nm and 1 nm optical slice linewidths, which features an EVM of 4.5% and 8.87% respectively.

In addition, Figure 6 shows the constellations for a QPSK signal conveyed in xPol with 0.1 nm and 1 nm optical slice linewidths onto 3.5 GHz. The measured EVM was 3.5% and 23% for optical slices linewidths of 0.1 nm and 1 nm respectively. Also, Figure 6 shows the constellations for a 64QAM signal transported in yPol with optical slices of 0.1 nm and 1 nm linewidths resulting in an EVM of 6% and 28.8% respectively. These results are in concordance with the bandwidth measurement shown in Figure 4 and demonstrate that the EVM increases, as the optical slice linewidth increases. Note that for an optical slice of 1nm, the information transported on 3.5 GHz, the constellation can barely be identified. In this scenario, wider optical slices significantly affect higher multilevel modulations, preventing tolerable signal quality from being obtained.

Figure 7 shows the EVM measurements results as a function of the optical slice linewidth for QPSK and 64QAM transported onto 1.7 GHz and 3.5 GHz. As observed in the constellations shown in Figures 5 and 6, notice that the degradation depends on the optical slice and on the radio frequency signal. However, it should be pointed out that the modulation format does not impact on the signal quality as the radio frequency does.

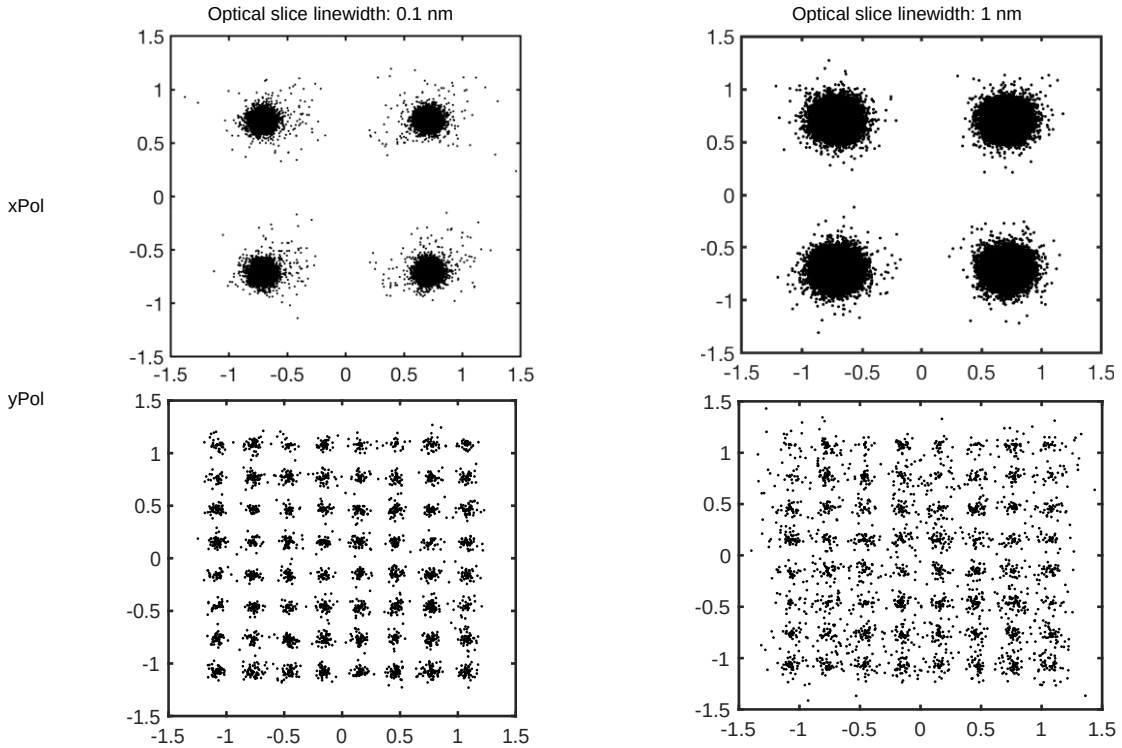

Figure 5. Experimental results: Measured constellations for a QPSK and 64QAM signal at 1.7 GHz after propagation on 10 km optical link. Source: Own elaboration.

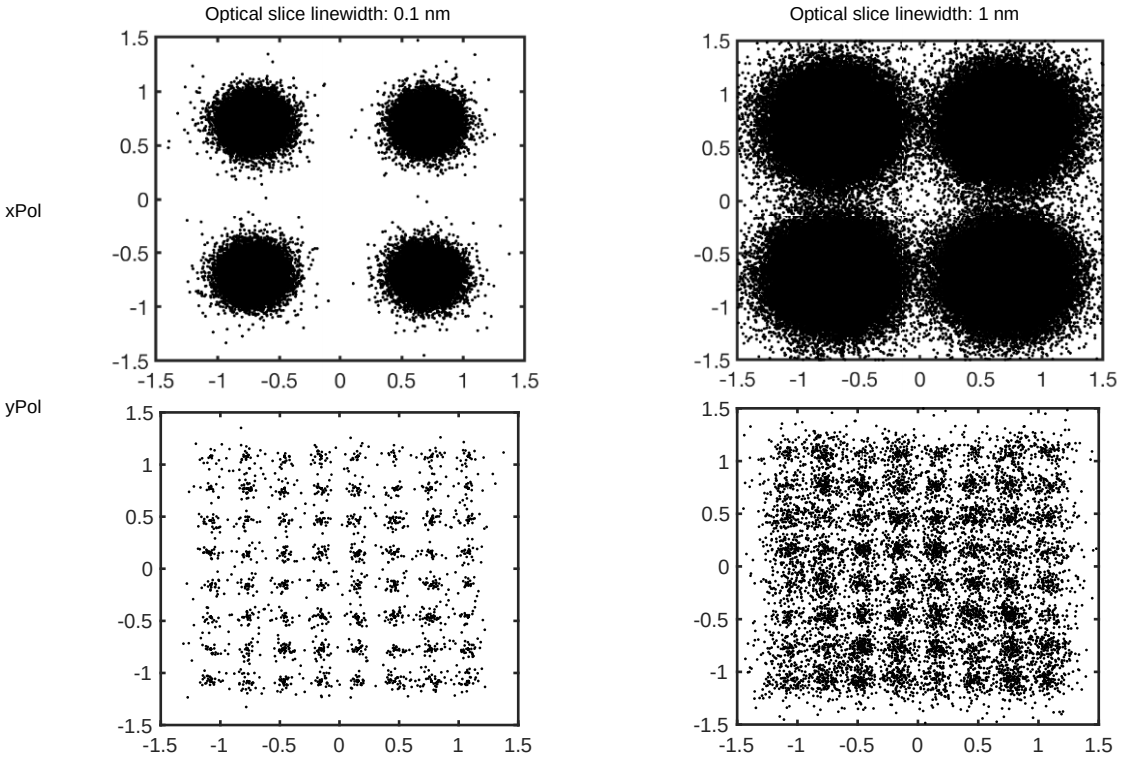

Figure 6. Experimental results: Measured constellations for a QPSK and 64QAM signal at 3.5 GHz after propagation on 10 km optical link. Source: Own elaboration.

Thus, whilst the QPSK signal performed reasonably similar to the 64QAM signal in the two evaluated radio frequencies for optical slices narrower than 0.4 nm, the cumulative chromatic dispersion produced a noticeable increment of the measured EVM in both modulation formats to optical slices wider than 0.5 nm. The slight better performance of the QPSK signal comes from the greater sensitivity to noise of the 64QAM modulation format. Furthermore, no notable difference of the signal quality was found in both polarized components. Regarding the measured signal quality, the third Generation Partnership Project (3GPP) defined the maximum EVM values for 5G standard according to the modulation format deployed [23]. In this context, while the EVM limit for the QPSK modulation is 17.5%, the EVM limit for a 64QAM modulation is 8%. These limits are represented with dashed lines in Figure 7. Thus, in accordance with the QPSK limit of the 3GPP, a QPSK signal at 1.7 GHz does not undergo limitations within the evaluated optical slices whereas a QPSK signal at 3.5 GHz can be transported onto a maximum optical slice linewidth of 0.7 nm. Similarly, due to the stringent quality requirements imposed to the 64QAM signal, it can be conveyed onto a maximum optical slice of 0.8 nm when the radio frequency carrier is 1.7 GHz and 0.45 nm when the carrier is 3.5 GHz.

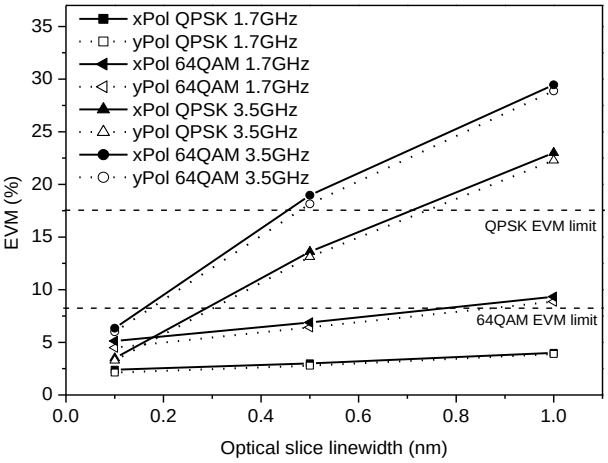

Figure 7. Experimental results: Measured EVM for dual polarized optical slices transporting QPSK and 64QAM modulation formats. Source: Own elaboration.

Beyond these slice linewidths for QPSK and 64QAM, the received signal quality does not fulfill the requirements of the 3GPP for 5G networks. These results suggest that dispersion compensation is required in order to enable the use of wider optical slices.

3.2. Simulation results

A set of conducted simulations of the layout shown in Figure 1 was executed in Optisystem in order to evaluate the EVM at longer fiber spams. The simulations included 15 MBauds QPSK and 64 QAM signals, optical propagation of up to 50 km. The configured optical slices were 0.1 nm and 0.3 nm as optical slices wider that 0.45 nm did not show a good experimental performance, particularly for 64QAM signals at 3.5 GHz, as seen above. Likewise, we noticed limitations of the software to sample bandwidths wider than 0.4 nm due to the reduction of the sample rate as the bandwidth was increased. In such a context, we observed that the conducted simulations for 0.1 nm match properly the experimental performance of the setup, as seen by comparing the results found for 0.1 nm in Figure 7 with the results shown in Figure 8.

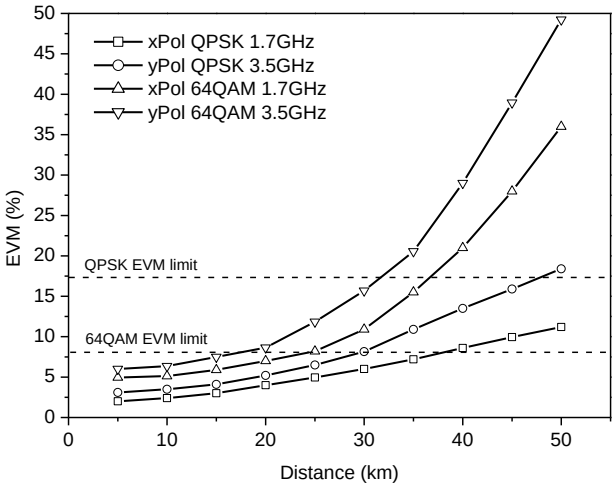

Figure 8. Modeling results: EVM as a function of the distance for a 0.1 nm optical slice linewidth. Source: Own elaboration.

Figure 8 shows the obtained results for an optical slice of 0.1 nm. It is observed that the obtained EVM depends on the distance due to the optical attenuation but also depends on the radio frequency carrier due to the effective modulation bandwidth derived from the chromatic dispersion effect accumulated by the subcarrier through the fiber propagation. In particular, the QPSK signal at 1.7 GHz provided the lowest EVM for 0.1 nm slice linewidth. The EVM increased, as the radio frequency was higher for each modulation. Taking into account the EVM limit defined above, it is observed that the proposed approach enables a fiber transmission of roughly 50 km for a QPSK signal at 3.5 GHz whereas distances longer than 50 km can be covered by the same modulation format at 1.7 GHz.

For the 64QAM signal, 25 km can be achieved with a carrier frequency of 1.7 GHz, and up to 16 km can be covered with a carrier frequency of 3.5 GHz. The modeling results depicted in Figure 9 for a 0.3 nm optical slice linewidth show that the QPSK radio signals at 1.7 GHz does not reach the EVM limit, therefore such signal can be propagated on a fiber spam longer than 40 km. Correspondingly, the QPSK signal at 3.5 GHz fulfills the EVM requirements at distances shorter than 32 km. Similarly, the 64QAM signals at 1.7 GHz and 3.5 GHz can be supported on a maximum fiber length of 15 km and 10 km respectively.

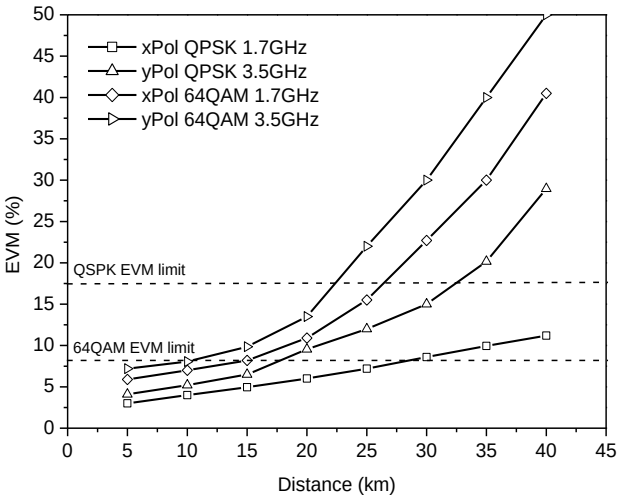

Figure 9. Modeling results: EVM as a function of the distance for a 0.3 nm optical slice. Source: Own elaboration.

In general, these results evidence a reduction of the reachable fiber length propagation due to the penalties caused by the chromatic dispersion on digitally modulated signals transported onto wider optical slices on both polarization components.

4. Conclusions

This paper presented and demonstrated an approach based on optical slicing and dual polarization for the transport of radio over fiber signals in the C-RAN of a 5G network. The approach aims at providing a solution for the transport of services in small cell deployments in order to support continuous cell densification for future mobile networks.

A mathematical description of the transfer function for the dual polarized optical slicing based on optical filtering and a broadband optical source was presented. In this a context and based on the conducted measurements, a modulation bandwidth of up to 3.7

GHz was found for a 0.1nm optical slice, such electrical bandwidth is reduced as the linewidth of the optical slice increases and the distance is longer due the effect imposed by the chromatic dispersion of the fiber. It was also observed that the optical power available per channel decreases as the optical slice linewidth increases. Thus, the quality of the received signal relies on the optical power and the accumulated chromatic dispersion of the link. The obtained outcomes confirmed that QPSK and 64QAM satisfy the EVM requirement within optical slices as wide as 1 nm transported at 1.7 GHz. However, radio frequency carriers at 3.5 GHz demand narrower optical slices of 0.3 nm and 0.18 nm for QPSK and 64QAM respectively in order to fulfill the signal quality requirements.

For both modulation formats, no substantial difference concerning the quality based on the polarization component was found. The simulation results envisage the operation of the proposed system at longer optical links. In this context, we found that a dual polarized optical slice system at 3.5 GHz across 50 km is possible using QPSK modulation onto an optical slice of 0.1 nm. For a 0.3 nm optical slice the reachable distance in which the EVM limit is fulfilled is reduced to 32 km. Overall, the outcomes shown in this paper demonstrates the feasibility of the approach in terms of the offered capacity and distance required for the deployment of next generation mobile networks. It is important to point out that the experimental results and the conducted simulations did not neither include dispersion compensation techniques nor optical amplification processes. By doing so, the capacity and reach of the proposed approach can be further improved.

Funding

Not applicable.

Autor Contributions

G. A. Puerto Leguizamón: Data Curation, Formal Analysis, Investigation, Methodology, Validation, Writing of Original Draft, Writing-Review, Editing. C. A. Suárez Fajardo: Data Curation, Formal Analysis, Investigation, Methodology, Validation, Writing of Original Draft, Writing-Review, Editing

Conflicts of Interest

Not applicable.

Institutional Review Board Statement

Not applicable.

Informed Consent Statement

Not applicable.

References

[1] B. Agarwal, M. A. Togou, M. Marco, G. -M. Muntean, “A Comprehensive Survey on Radio Resource Management in 5G HetNets: Current Solutions, Future Trends and Open Issues,” in *IEEE Communications Surveys & Tutorials*, vol. 24, no. 4, pp. 2495-2534, Fourthquarter 2022, doi: https://doi.org/10.1109/COMST.2022.3207967

[2] J. Brenes *et al*., "Network slicing architecture for SDM and analog-radio-over-fiber-based 5G fronthaul networks,” in *Journal of Optical Communications and Networking*, vol. 12, no. 4, pp. B33-B43, April 2020, doi: https://doi.org/10.1364/JOCN.381912

[3] X. Liu, “Enabling Optical Network Technologies for 5G and Beyond,” in Journal of Lightwave Technology, vol. 40, no. 2, pp. 358-367, 2022, doi: https://doi.org/10.1109/JLT.2021.3099726

[4] L. M. P. Larsen, H. L. Christiansen, S. Ruepp and M. S. Berger, “Toward Greener 5G and Beyond Radio Access Networks—A Survey,” in *IEEE Open Journal of the Communications Society*, vol. 4, pp. 768-797, 2023, doi: https://doi.org/10.1109/OJCOMS.2023.3257889

[5] I. Coddington et al., “Dual-comb spectroscopy,” *Optica*, vol. 3, no. 4, Apr. 2016, Art. no. 414, doi: https://doi.org/10.1364/OPTICA.3.000414

[6] J. Lin, H. Sepehrian, Y. Xu, L. A. Rusch and W. Shi, “Frequency Comb Generation Using a CMOS Compatible SiP DD-MZM for Flexible Networks,” in *IEEE Photonics Technology Letters*, vol. 30, no. 17, pp. 1495-1498, 2018, doi: https://doi.org/10.1109/LPT.2018.2856767

[7] M. Mazur *et al*., “High Spectral Efficiency Coherent Superchannel Transmission With Soliton Microcombs,” in *Journal of Lightwave Technology*, vol. 39, no. 13, pp. 4367-4373, July1, 2021, doi: https://doi.org/10.1109/JLT.2021.3073567

[8] H. Othman, X. Ouyang, C. Antony, F. Smyth and P. D. Townsend, “Spectrally-Sliced Coherent Receiver Utilizing a Gain-Switched Optical Frequency Comb,” in *Journal of Lightwave Technology*, vol. 41, no. 16, pp. 5262-5274, 2023, doi: https://doi.org/10.1109/JLT.2023.3256180

[9] M. Imran, P. M. Anandarajah, A. Kaszubowska-Anandarajah, N. Sambo, L. Potí, "A Survey of Optical Carrier Generation Techniques for Terabit Capacity Elastic Optical Networks," in *IEEE Communications Surveys & Tutorials*, vol. 20, no. 1, pp. 211-263, Firstquarter 2018, doi: https://doi.org/10.1109/COMST.2017.2775039

[10] Hu, Hao and Oxenløwe, "Chip-based optical frequency combs for high-capacity optical communications", *Nanophotonics*, vol. 10, no. 5, 2021, doi: https://doi.org/10.1515/nanoph-2020-0561

[11] C. Browning, D. Dass, P. Townsend, X. Ouyang, "Orthogonal Chirp-Division Multiplexing for Future Converged Optical/Millimeter-Wave Radio Access Networks," in *IEEE Access*, vol. 10, pp. 3571-3579, 2022, doi: https://doi.org/10.1109/ACCESS.2021.3137716

[12] Lundberg, L., Mazur, M., Mirani, A. *et al.* "Phase-coherent lightwave communications with frequency combs", *Nat Commun* , 2020, doi: https://doi.org/10.1038/s41467-019-14010-7

[13] C. Quevedo-Galán, V. Durán, A. Rosado, A. Pérez-Serrano, J. M. G. Tijero, and I. Esquivias, "Gain-switched semiconductor lasers with pulsed excitation and optical injection for dual-comb spectroscopy," *Opt. Express*, vol. 28, 33307-33317, 2020, doi: https://doi.org/10.1364/OE.404398

[14] C. Browning *et al.*, "Gain-Switched Optical Frequency Combs for Future Mobile Radio-Over-Fiber Millimeter-Wave Systems," in *Journal of Lightwave Technology*, vol. 36, no. 19, pp. 4602-4610, 2018, doi: https://doi.org/10.1109/JLT.2018.2841365

[15] M. Sun *et al.*, "Spectrally Efficient Direct-Detection THz Communication System Enabled by Twin Single-Sideband Modulation and Polarization Division Multiplexing Techniques," *2022 Asia Communications and Photonics Conference (ACP)*, Shenzhen, China, 2022, pp. 53-56, doi: https://doi.org/10.1109/ACP55869.2022.10088517

[16] C. Li, X. Chen, Z. Chen and F. Zhang, "Capacity Increase in Dual-polarization Nonlinear Frequency Division Multiplexing Systems with Probabilistic Shaping," *2021 Opto-Electronics and Communications Conference (OECC)*, 2021, doi: https://doi.org/10.1364/OECC.2021.W1B.2

[17] Y. Cai *et al.*, "Spectrally Efficient PDM-Twin-SSB Direct-Detection THz System Without Active Polarization Control," in *IEEE Photonics Technology Letters*, vol. 35, no. 15, pp. 838-841, 2023, doi: https://doi.org/10.1109/LPT.2023.3275921

[18] Y. Lin *et al.*, "Narrow Linewidth Hybrid InP-TriPleX Photonic Integrated Tunable Laser Based on Silicon Nitride Micro-ring Resonators," *2018 Optical Fiber Communications Conference and Exposition (OFC)*, San Diego, CA, USA, 2018, pp. 1-3.

[19] Almae Technologies, "10G C-band DWDM EML laser chip," 2023. [Online]. Available: https://almae-technologies.com/wp-content/uploads/2020/12/AEM2001-10-C1-15XX.pdf

[20] A. R. Totović, J. V. Crnjanski, M. M. Krstić and D. M. Gvozdić, "Numerical Study of the Small-Signal Modulation Bandwidth of Reflective and Traveling-Wave SOAs," in *Journal of Lightwave Technology*, vol. 33, no. 13, pp. 2758-2764, 2015. doi: https://doi.org/10.1109/JLT.2015.2412252

[21] C. Dragone, "An N*N optical multiplexer using a planar arrangement of two-star couplers," in *IEEE Photonics Technology Letters*, vol. 3, no. 9, pp. 812-815, Sept. 1991, doi: https://doi.org/10.1109/68.84502

[22] J. Song *et al.*, "Low aberration concave grating for re-configurable optical add/drop multiplexer applications," *2011 International Topical Meeting on Microwave Photonics jointly held with the 2011 Asia-Pacific Microwave Photonics Conference*, Singapore, 2011, doi: https://doi.org/10.1109/MWP.2011.6088684

[23] ETSI, "5G, NR, Base Station (BS) radio transmission and reception (3GPP TS 38.104 version 15.5.0 Release 15)," 2019. [Online]. Available: https://www.etsi.org/deliver/etsi_ts/138100_138199/138104/15.05.00_60/ts_138104v150500p.pdf